Magnetic scanning tunneling microscopy with a two-terminal nonmagnetic tip: Quantitative results

T. P. Pareek and Patrick Bruno
Max-Planck-Institute für Mikrostrukturphysik, Weinberg 2, D-06120 Halle, Germany
(Received 31 July 2000; published 5 April 2001)

We report numerical simulation results of a recently proposed [P. Bruno, Phys. Rev. Lett **79**, 4593 (1997)] approach to perform magnetic scanning tunneling microscopy with a two terminal nonmagnetic tip. It is based upon the spin asymmetry effect of the tunneling current between a ferromagnetic surface and a two-terminal nonmagnetic tip. The spin asymmetry effect is due to the spin-orbit scattering in the tip. The effect can be viewed as a Mott scattering of tunneling electrons within the tip. To obtain quantitative results we perform numerical simulations within the single-band tight-binding model, using the recursive Green's-function method and the Landauer-Büttiker formula for conductance. A model has been developed to take into account the spin-orbit scattering off the impurities within the single-band tight-binding model. We show that the spin-asymmetry effect is most prominent when the device is in the quasiballistic regime and the typical value of spin asymmetry is about 5%.

DOI: 10.1103/PhysRevB.63.165424 PACS number(s): 68.37.Ef, 73.40.Gk, 75.70.Rf, 75.60.Ch

I. INTRODUCTION

Imaging the magnetic structures of surfaces down to the atomic level is a major goal of surface magnetism. Magnetic scanning tunneling microscopy (MSTM) provides a way to image magnetic domains on the surface. In the conventional approach, magnetic sensitivity of the tunneling current has been based upon the spin-valve effect,[1] the tunneling current between two ferromagnets separated by a tunnel barrier depend on the relative orientation of the magnetizations of the ferromagnets. In this approach a magnetic tip has to be used. The experimental realization of magnetic scanning tunneling microscopy based on the spin-valve effect was realized by Wiesendanger *et al.*,[2] who investigated a Cr(001) surface with a ferromagnetic CrO_2 tip, their observation confirmed the model of topological antiferromagnetism between ferromagnetic terraces separated by monoatomic steps. They measured a spin asymmetry of the order of 20%. Recently this method has been used to image magnetic domains.[3–6] It was shown that, by periodically changing the magnetization of tip, it is possible to separate the spin-dependent tunnel current from the topographic dependent current and hence the magnetic structure of surface can be recorded. Using this method, Wulfhekel *et al.*[3] studied magnetic domain structure on single crystalline Co(0001) surface and polycrystalline Ni surface. In Refs. 4–6, a two-dimensional antiferromagnetic structure of Mn atoms on tungsten(110) surface was investigated. It was shown that the spin-polarized tunneling current is sensitive to the magnetic superstructure, and not to the chemical unit cell.[4]

However, the MSTM with a magnetic tip has the drawback that the magnetostatic interaction between the tip and magnetic sample cannot be avoided, which is likely to influence the domain structure. In view of this, an alternative approach was recently proposed to perform the magnetic scanning tunneling microscopy with a two terminal nonmagnetic tip.[7] It is based upon Mott's spin-asymmetry effect in scattering caused by disorder.[8] It was shown that due to spin-orbit coupling, the tunnel conductance between the ferromagnetic surface and one of the tip terminals depends on the orientation of magnetization. Because of the spin-orbit interaction, the intensity of the scattered beam depends on the orientation of the spin-polarization axis of the incidents electrons, i.e., it is sensitive to the spin component perpendicular to the scattering plane. In other words, tunnel conductance is spin asymmetric. However, to observe this spin asymmetry effect, caused by Mott scattering, a three terminal device is a prerequisite. Due to the Casimir-Onsager symmetry relation the conductance of a two-terminal device has to be symmetric with respect to magnetic field (in our case, spin plays the role of magnetic field since, as far as time reversal properties are concerned, ''spin'' and ''magnetic'' fields are equivalent), this is a requirement imposed by the underlying microscopic time reversal symmetry. However, in case of three terminal device, there is no such restriction on the conductance; rather, a more generalized symmetry relation exists involving all terminals, as shown by Büttiker.[9] Hence, to perform magnetization sensitive scanning tunneling microscopy with a nonmagnetic tip, it is necessary to use a two terminal tip.[7]

In this work we report numerical simulation results of the three terminal STM device within the single-band tight-binding model, using the recursive Green-function method and the Landauer-Büttiker formula for conductance.[10] We have developed a model to take into account spin-scattering within the single-band tight-binding model.

This paper is organized as follows. In Sec. II we introduce the single-band tight-binding model including the spin-orbit interaction and the three terminal STM device. Section III briefly describes the method of calculation. In Sec. IV we present some numerical results and discussion.

II. MODEL AND METHOD

A cross section of the system in the *xy* plane, for the calculation of spin sensitivity of the proposed two terminal nonmagnetic tip, is shown in Fig. 1. The system consists of

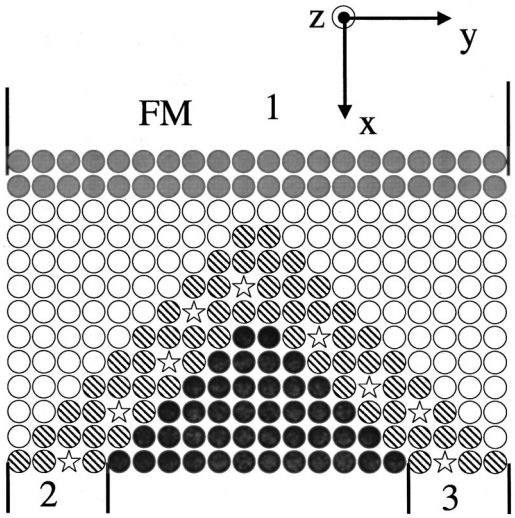

FIG. 1. Cross section of tip geometry shown in the xy plane. Gray circles denote the ferromagnetic sample; the empty circles depict vacuum; black circles correspond to insulating sites; and the rest correspond to metallic sites (hatched circles) and the impurities (stars) in the tip. This figure shows one typical realization of the disorder.

three regions, (i) the ferromagnetic lead (labeled 1 in Fig. 1), (ii) the central region, and (iii) the two nonmagnetic terminals (labeled as 2 and 3 in Fig. 1). The central region is composed of an insulating tip, such as those routinely used to perform atomic force microscopy, coated on two opposite faces by a thin metallic film. The metallic coating has thickness d. This is shown in the central region where the empty circles depict vacuum, black circles correspond to insulating sites, and the rest correspond to metallic sites (hatched circles) and the impurities (stars). Between the ferromagnetic surface (gray circles in Fig. 1) and the tip there is a vacuum layer of one lattice spacing (empty circles in Fig. 1). The tip is placed symmetrical with respect to the xz plane. Current flows along the two faces of the tip, which makes an angle of ± 45 degrees with the x axis. The structure shown in Fig. 1 consists of three semi-infinite leads ($-\infty \leqslant i \leqslant 1$ and $N_x+1 \leqslant i \leqslant \infty$) separated by the tip region $1 \leqslant i \leqslant N_x$. The thickness of the metallic coating on the tip is da where a is the lattice constant and the cross section of the system is $(N_y a \times N_z a)$, where N_y and N_z are the number of sites along the y and z axes. For numerical calculation we have taken $N_y = N_z = 20$, $N_x = 10$, and the metallic coating on the tip has a thickness of four lattice spacings, i.e., $d=4$, as shown in Fig. 1.

We model the system shown in Fig. 1 as a single-band tight-binding Hamiltonian with nearest neighbor hopping parameter t. To obtain the appropriate form of single-band tight-binding Hamiltonian including spin-orbit interaction, we discretize the following single-band Hamiltonian in continuum, on a simple-cubic lattice:

$$H = \frac{\hat{P}^2}{2m^*} + V(\mathbf{r}) + \frac{\Delta}{2}\vec{\mu}(\mathbf{r}) \cdot \vec{\sigma} + \lambda (\nabla V(\mathbf{r}) \times \vec{\sigma}) \cdot \hat{P}, \quad (1)$$

where the first two terms are the usual kinetic and potential energies while the third and fourth terms represent exchange and spin-orbit interaction, respectively; m^* is the effective mass of an electron; Δ is the exchange splitting; $\vec{\mu}$ is a unit vector in the direction of magnetization of FMs and is given by $(\cos\phi \sin\theta, \sin\phi \sin\theta, \cos\theta)$; $\vec{\sigma}$ is the Pauli operator; and $\hat{P}$ is the momentum operator. The discretized form of the Hamiltonian reads

$$H = \sum_{\mathbf{r},\sigma,\sigma'} \left(\varepsilon_{\mathbf{r}} \delta_{\sigma\sigma'} + \frac{\Delta_{\mathbf{r}}}{2} \vec{\mu}_{\mathbf{r}} \cdot \vec{\sigma}_{\sigma\sigma'} \right) c^{+}_{\mathbf{r},\sigma} c_{\mathbf{r},\sigma'} + t \sum_{\langle \mathbf{r},\mathbf{r}' \rangle \sigma} c^{+}_{\mathbf{r},\sigma} c_{\mathbf{r}',\sigma} + H_{\mathrm{so}}, \quad (2)$$

where H_{so} is expressed as

$$H_{\mathrm{so}} = -i\alpha_{\mathrm{so}} \times \sum_{\mathbf{r},\sigma,\sigma',i,j,k,\nu\gamma} \nu\gamma \Delta\varepsilon_{\mathbf{r}+\gamma\mathbf{a}_k, \mathbf{r}+\nu\mathbf{a}_j} c^{\dagger}_{\mathbf{r},\sigma} c_{\mathbf{r}+\nu\mathbf{a}_j+\gamma\mathbf{a}_k} \sigma^{i}_{\sigma\sigma'} \epsilon_{ijk}. \quad (3)$$

Here $c^{+}_{\mathbf{r},\sigma}$ is the creation operator of an electron with spin σ at site $\mathbf{r}$, $\varepsilon_{\mathbf{r}}$ is the on-site energy, and $\Delta\varepsilon_{\mathbf{r}+\gamma\mathbf{a}_k, \mathbf{r}+\nu\mathbf{a}_j} = \varepsilon_{\mathbf{r}+\gamma\mathbf{a}_k} - \varepsilon_{\mathbf{r}+\nu\mathbf{a}_j}$, $\mathbf{a_i}$ is the lattice basis vector along axis i, $\sigma^{i}_{\sigma\sigma'}$ denotes the Pauli matrix elements, and α_{so} is the dimensionless spin-orbit parameter. The dummy indice $\nu\gamma$ takes the values $\pm$. The summation $\langle \mathbf{r},\mathbf{r}' \rangle$ runs over nearest neighbor sites. The symbol $\epsilon_{\mathbf{ijk}}$ is the Levi-Civita's totally antisymmetric tensor, where ijk label the three coordinate axis.

The tight-binding parameters in Eqs. (2) and (3) are related with the parameters in Eq. (1) in the following way:

$$t = -\frac{\hbar^2}{2m^* a^2}, \quad (4)$$

$$\alpha_{\mathrm{so}} = \frac{\lambda\hbar}{a^2}. \quad (5)$$

The above tight-binding model includes two factors: spin-dependent band structure and spin-independent disorder. The band structure takes into account the difference in the density of states and the Fermi velocity between the two spin components in the ferromagnet. The disorder represents the structural defects in the real STM tip and is the source of spin-orbit scattering; it also takes the form of spin independent random variation in the atomic on-site energies. In presence of disorder, the spin-orbit coupling term causes hopping along the diagonal and is the source of spin-flip scattering. In this sense, this model is equivalent to the next-nearest-neighbor (nnb) tight-binding model, except that in the usual nnb tight-binding model, hopping amplitude to the next-nearest neighbor is fixed while in our model it depends on disorder strength and the spin of the electron. Hence within this model spin-relaxation length is determined by disorder strength.

III. THEORY

As shown in Fig. 1, the ferromagnet and the left and right faces of the tip, are connected to three reservoirs at chemical potentials V_1, V_2, and V_3, respectively. Let I_1, I_2, and I_3 be the corresponding incoming currents in the three terminals.[9,10]

The currents are related to potentials by

$$I_p = \sum_{q \neq p} G_{pq}(V_p - V_q). \tag{6}$$

The above expression is gauge invariant and the currents conservation law $\Sigma_i I_i = 0$ requires that $G_{pq} = G_{qp}$ be satisfied.

The calculation of the conductance of the structure is based upon the nonequilibrium Green's-function formalism.[11,12] When applied to the multiterminal ballistic mesoscopic conductor, we obtain the following result for the conductance:[10]

$$G_{pq} = \frac{e^2}{h} \mathrm{Tr}[\Gamma_q G^R \Gamma_p G^A]. \tag{7}$$

Here p and q enumerates the three terminals, and the upper indices R and A refer to the retarded and advanced Green function of the whole structure, taking leads into account. Here $\Gamma_{p(q)}$ is the self-energy function for the isolated ideal leads which are given by $\Gamma_{p(q)} = t^2 A_{p(q)}$, where $A_{p(q)}$ is the spectral density in the respective lead when it is decoupled from the structure. The trace is over space and spin degrees of freedom, and all the matrices in Eq. (4) are of size $(2N_y \times N_z, 2N_y \times N_z)$, where N_y and N_z are a number of sites along the y and z directions and the factor of 2 takes into account the spin degree of freedom. All the quantities in the above equations are evaluated at the Fermi energy. To calculate the required Green function we use the well-known recursive Green's-function method.[13]

IV. RESULTS AND DISCUSSION

In this section, we present numerical results for a system of cross section (20×20) in the yz plane and a length of 10 lattice spacing along the x direction. The number of metallic layers on the tip, i.e., d in Fig. 1 is taken to be four lattice spacings. The hopping parameter, t, is the same for all pairs and set to -1 for numerical calculation. The on-site energies in the leads and on the metal coating on the tip is set to be zero, while in the vacuum layer it is $\epsilon_{\mathrm{vac}} = 4.0|t|$, and in the insulating region in the tip it is $\epsilon_{\mathrm{ins}} = 10.0|t|$. The Fermi level throughout the calculation is kept fixed at $\epsilon_f = 3|t|$ above the bottom of the band. For disorder, we consider the Anderson model in which a random on-site energy, characterized by square distribution of width W, is added to the on-site energy of a perfect case. In our case, disorder is added only in the metallic coating on the tip; everywhere else the system is perfect.

Before we go over to the discussion of our results, we briefly mention the correspondence between the physical parameters and the model parameters. The relevant physical parameters are the mean free path, spin-relaxation length Fermi energy, and spin polarization of the ferromagnet at the Fermi level while the model parameters are on-site energy, hopping energy, exchange splitting, and spin-orbit coupling parameters. Physical parameters are related to the model parameters in the following way:

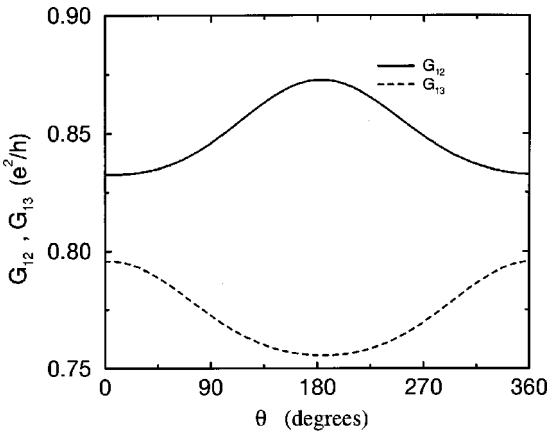

FIG. 2. Conductance (G_{12} and G_{13}) versus θ plot for the two terminals for a fixed value of $\phi = 90$. The other parameters chosen for this figure are $\epsilon_f = 3.0|t|$, $\Delta = 2.4|t|$, $\alpha_{so} = 0.02$, and $W = 1|t|$.

$$l_m = \frac{|t|}{\pi} \sqrt{\frac{\epsilon_f}{|t|}} \frac{1}{N_{3D}(\epsilon_f)\langle (V - \overline{V})^2 \rangle_c} a, \tag{8}$$

$$l_{\mathrm{so}} = l_m \sqrt{\frac{\tau_{\mathrm{so}}}{\tau_m}} \equiv \frac{3 l_m |t|}{2|\alpha_{\mathrm{so}}|\epsilon_f}, \tag{9}$$

$$P = \frac{N^{\uparrow}(\epsilon_f) - N^{\downarrow}(\epsilon_f)}{N^{\uparrow}(\epsilon_f) + N^{\downarrow}(\epsilon_f)} \equiv \frac{\sqrt{\epsilon_f + \Delta} - \sqrt{\epsilon_f - \Delta}}{\sqrt{\epsilon_f + \Delta} + \sqrt{\epsilon_f - \Delta}}, \tag{10}$$

where l_m, l_{so}, and P are the elastic mean free path, spin relaxation length, and spin polarization of the ferromagnet, respectively. Here a is lattice spacing and $\langle \cdots \rangle_c$ represents the configuration averaging. Other symbols have the same meaning as defined in Sec. II. Below we present some numerical results for one typical realization of the disorder. We have not performed disorder averaging.

In Fig. 2 we have plotted the conductance G_{12} and G_{13} as a function of magnetization angle θ with respect to the z axis. We rotate the magnetization in the yz plane such that the magnetization is always perpendicular to the x axis, or in other words, the angle ϕ does not change and has a fixed value of 90°. To be specific, when $\theta = 0$ and $\phi = 90°$, magnetization is parallel to the z axis, while for $\theta = 90°$ and $\phi = 90°$ the magnetization is parallel to the y axis. We have taken $\epsilon_f = 3|t|$, $\alpha_{\mathrm{so}} = 0.02$, and $\Delta = 2.4|t|$, and the Anderson disorder strength is $W = 1|t|$. This set of parameters corresponds to a mean free path of $l_m = 80a$, spin relaxation length of $l_{so} = 25 l_m$, and polarization is $P = 50\%$. We notice that the conductance shows approximately $\cos(\theta)$ as a function of angle, which is expected since, in our geometry, the tip is placed symmetrically to the xz plane. However, because of disorder, the effective axis in the system does not coincide

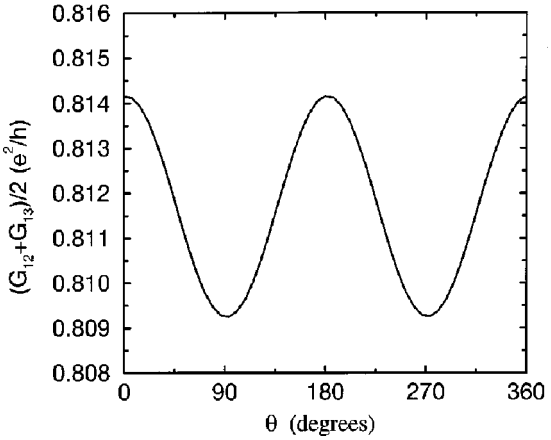

FIG. 3. Plot of the average two-terminal conductance $(G_{12}+G_{13})/2$ vs θ. The other parameters are the same as those in Fig. 2.

with the chosen spin quantization axis, i.e., z axis; and also since the structure considered is three dimensional so the scattering plane is not fixed, hence the conductance variation with magnetization angle does not show an exact cosine behavior. Also we notice that the variation of G_{13} is opposite that of G_{12}. This is in agreement with the underlying microscopic time-reversible symmetry which requires that the two terminal conductance should be symmetric under time reversal. To verify this point, we have plotted in Fig. 3 the sum of $(G_{12}+G_{13})/2$, where we see that the two terminal conductance is symmetric with respect to magnetization angle θ. Also, the magnitude of oscillation is much smaller than either G_{12} or G_{13}. This is due to the fact that the variation of G_{12} or G_{13} with θ is of first order with respect to the spin-orbit coupling, whereas the variation of $G_{12}+G_{13}$ is of second order with respect to spin-orbit coupling. Actually, the latter can be viewed as related to the anisotropic magnetoresistance of ferromagnets, whereas the former is related to the extraordinary Hall effect.

In Fig. 4 we plot spin asymmetry as a function of the polarization of the ferromagnet for terminal 2. We have defined the spin asymmetry as

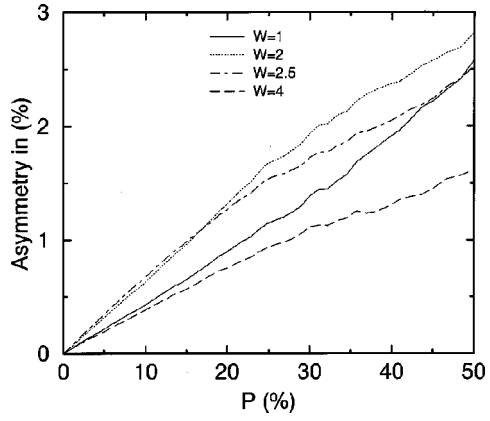

FIG. 4. Spin asymmetry A, as a function of polarization for different disorder strengths. The other parameters are $\epsilon_f=3.0|t|$ and $\alpha_{so}=0.02$.

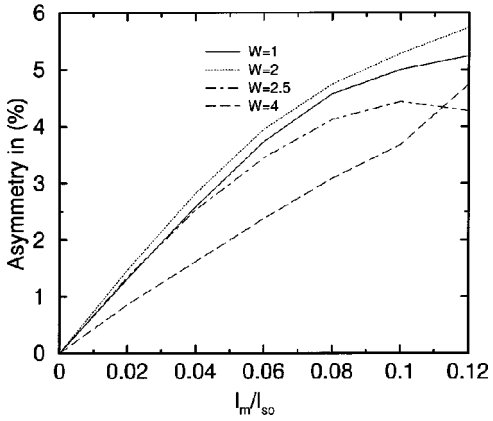

FIG. 5. Spin asymmetry A, as a function of l_m/l_{so} for different disorder strengths. The other parameters are $\epsilon_f=3.0|t|$ and $\Delta=2.4|t|$. The corresponding value of polarization is 50%.

$$A=\frac{G_{12}^{\max}-G_{12}^{\min}}{G_{12}^{\max}+G_{12}^{\min}}, \tag{11}$$

where to find $G_{12}^{\max}$ and $G_{12}^{\min}$ we generate a curve, as shown in Fig. 3, for each set of parameters, and from those points we get the corresponding maximum and minimum values. This is necessary since the variation of conductance with magnetization angle does not follow exact cosine behavior, and the maxima and minima need not to occur exactly at zero and π, respectively. We have fixed Fermi energy at $\epsilon_f=3|t|$ and $\alpha_{so}=0.02$. Different curves in Fig. 4 corresponds to disorder strengths $W=1|t|$ (solid line), $W=2|t|$ (dotted line), $W=2.5|t|$ (dot-dashed line), and $W=4|t|$ (dashed line). The corresponding mean free paths are, respectively, $80a$, $10a$, $6a$, and $3a$. Although all these curves correspond to different mean free paths, the ratio l_{so}/l_m is the same for all the curves and is equal to 25 since this ratio is determined by Fermi energy and spin-orbit coupling strength, which are kept fixed here. We see that for a fixed disorder strength the spin asymmetry increases linearly with the polarization, or in other words, spin asymmetry is directly proportional to the polarization of the ferromagnet. However, for a fixed polarization value, spin asymmetry shows a nonmonotonic behavior. As we increase disorder strength, spin asymmetry first increases and then starts decreasing. This shows that the spin asymmetry is maximum when the system is in the quasiballistic regime, since the multiple scattering destroys the spin asymmetry effect. This is clearly visible in Fig. 4 where spin asymmetry is maximum for a fixed value of polarization at a disorder strength $W=2|t|$ corresponding to a mean free path of $10a$, while it is minimum for $W=4|t|$ corresponding to a mean free path of $3a$ lattice spacings. The order of magnitude of spin asymmetry is 5%, which is in good agreement with the prediction in Ref. 7.

In Fig. 5 we have studied the behavior of spin asymmetry as a function of spin-orbit coupling parameter α_{so}. The other parameters are the same as in Fig. 4. We notice that the spin-asymmetry shows a linear behavior for small values of $\alpha_{so}\leqslant 0.03$. For larger α_{so}, the linear behavior is no longer seen because for a fixed disorder (i.e., fixed l_m), as we in-

crease α_{so}, correspondingly, l_{so} (i.e., spin-relaxation path) decreases. Hence the higher-order effect in spin-orbit coupling starts dominating, so we no longer observe a linear behavior. Also, we see that for a fixed α_{so}, spin asymmetry shows a maximum at a disorder strength of around $W=2|t|$. This is in harmony with the results presented in Fig. 4. The typical value of spin asymmetry is of the order of 5%. So from the results of Figs. 4 and 5 we can say with confidence that the efficiency of the proposed three terminal STM device would be maximum when the device operates in the quasiballistic regime.

In summary, we have developed a model to take into account spin-orbit scattering within the single-band tight-binding model. Using this model, we have done numerical calculations of magnetic scanning tunneling microscopy with a nonmagnetic tip. The order of magnitude of the spin asymmetry is about 5%, which is in good agreement with the qualitative estimate given in Ref. 7 and the effect is maximum when the device operates in the quasiballistic regime. The spin asymmetry of the present effect is smaller than the one obtained in the spin-valve tunneling structures. However, it has some advantages. In particular, since the tip is nonmagnetic, it is insensitive to an external magnetic field. This allows one to study the domain structure as a function of the applied field. Furthermore, the problem of the magnetostatic interaction between the tip and the magnetic sample is avoided, which, in the case of a magnetic tip, would give rise to undesirable magnetic forces between the tip and the sample, which are likely to influence the domain structure. Another important advantage of this technique is that by measuring separately the currents I_2 and I_3 of the two tip terminals, and by combining them appropriately, one can separate the weak magnetic contrast from the dominant topographic contrast. The sum I_2+I_3 depends only on the topography, whereas the magnetic information is contained in the difference I_2+I_3. Besides all these advantages, it has an intrinsic limitation that the only in-plane components can be studied. Also, since multiple scattering diminishes the spin-asymmetry effect, it is necessary that the device operates in a quasiballistic regime. However, to construct such a tip would be experimentally challenging.

[1] M. Juliere, Phys. Lett. **54A**, 225 (1975); S. Maekawa and U. Gäfvert, IEEE Trans. Magn. **18**, 707 (1982); J.C. Slonczewski, Phys. Rev. B **39**, 6995 (1989).

[2] R. Wiesendanger, H.J. Güntherodt, G. Güntherodt, R.J. Gambino, and R. Ruf, Phys. Rev. Lett. **65**, 247 (1990); R. Wiesendanger, J. Magn. Soc. Jpn. **18**, 4 (1994).

[3] W. Wulfhekel and J. Kirschner, Appl. Phys. Lett. **75**, 1944 (1999).

[4] S. Heinze, M. Bode, A. Kubetzka, O. Pietzsch, X. Nie, S. Blügel, and R. Wiesendanger, Science **288**, 1805 (2000).

[5] O. Pietzsch, A. Kubetzka, M. Bode, and R. Wiesendanger, Phys. Rev. Lett. **84**, 5212 (2000).

[6] M. Bode, M. Getzlaff and R. Wiesendanger, Phys. Rev. Lett. **81**, 4256 (1998).

[7] P. Bruno, Phys. Rev. Lett. **79**, 4593 (1997).

[8] N.F. Mott, Proc. R. Soc. London, Ser. A **124**, 438 (1929).

[9] M. Büttiker, Phys. Rev. Lett. **57**, 1761 (1986); IBM J. Res. Dev. **32**, 317 (1988).

[10] S. Datta, *Electronic Transport in Mesoscopic Systems* (Cambridge University Press, Cambridge, 1995).

[11] L. P. Kadanoff and G. Baym, *Quantum Statistical Mechanics* (Benjamin, New York, 1962).

[12] L.V. Keldysh, Sov. Phys. JETP **20**, 1018 (1965).

[13] H.U. Baranger, D.P. DiVincenzo, R.A. Jalabert, and A.D. Stone, Phys. Rev. B **44**, 10 637 (1991).